Antimagnetic rotation and sudden change of electric quadrupole transition strength in ^{143}Eu

S. Rajbanshi [a], S. Roy [b], Somnath Nag [c,1], Abhijit Bisoi [a,2], S. Saha [b], J. Sethi [b], T. Bhattacharjee [d], S. Bhattacharyya [d], S. Chattopadhyay [a], G. Gangopadhyay [e], G. Mukherjee [d], R. Palit [b], R. Raut [f], M. Saha Sarkar [a], A.K. Singh [c], T. Trivedi [g], A. Goswami [a,*]

[a] *Saha Institute of Nuclear Physics, Kolkata 700 064, India*
[b] *Tata Institute of Fundamental Research, Mumbai 400005, India*
[c] *Indian Institute of Technology, Kharagpur 721302, India*
[d] *Variable Energy Cyclotron Center, Kolkata 700064, India*
[e] *University of Calcutta, Kolkata 700009, India*
[f] *UGC-DAE Consortium for Scientific Research, Kolkata 700098, India*
[g] *Guru Ghasidas Vishayavidyalaya, Bilaspur 495009, India*

A R T I C L E   I N F O

A B S T R A C T

Lifetimes of the states in the quadrupole structure in ^{143}Eu have been measured using the Doppler shift attenuation method and the parity of the states in the sequence has been firmly identified from polarization measurements using the Indian National Gamma Array. The decreasing trends of the deduced quadrupole transition strength $B(E2)$ with spin, along with increasing $J^{(2)}/B(E2)$ values before the band crossing, conclusively establish the origin of these states as arising from antimagnetic rotation. The abrupt increase in the $B(E2)$ values after the band crossing in the quadrupole band, a novel feature observed in the present experiment, may possibly indicate the crossing of different shears configurations resulting in the re-opening of a shears structure. The results are reproduced well by numerical calculations within the framework of a semi-classical geometric model.

© 2015 The Authors. Published by Elsevier B.V. This is an open access article under the CC BY license (http://creativecommons.org/licenses/by/4.0/). Funded by SCOAP^3.

It is well known that the deviation of a quantal system from spherical symmetry results in the observation of regular band-like structures in its excitation spectrum, with the excitation energy proportional to $I(I + 1)$, I being the quantized angular momentum of a state [1]. The deformed nuclei, found in specific mass regions of the periodic table [2,3], are the best examples of such quantum rotation. In a true sense it is the charge density that deviates from spherical symmetry which specifies the orientation of the system as a whole. The resulting sequence of rotational levels gives rise to a band structure where the states are connected through strong $E2$ transitions. The experimental signature of these bands is the observation of nearly constant electric quadrupole transition rates which are proportional to the square of the electric quadrupole moment operator [4].

Interestingly, similar regular sequences of quadrupole transitions have also been observed for nuclei with small quadrupole collectivity, but with different intrinsic properties compared to strongly deformed systems [5–7]. This type of excitation mechanism was first reported by Zhu et al. [8] from the spectroscopic investigation of the ^{100}Pd nucleus. These bands are characterized by decreasing electric quadrupole transition rates [$B(E2)$] with increasing spin [9–15]. The intriguing feature of the falling trend of the $B(E2)$ values of these sequences has been visualized as a new form of quantized rotation, known as antimagnetic rotation (AMR) and has been interpreted in the framework of a shears mechanism [16]. In this description the angular momentum is generated by the closing of the two blades of conjugate shears, produced by the valence particles (holes). These valence particles (holes) are initially aligned in time reversed orbits at the bandhead [16]. There is no net perpendicular component of the magnetic dipole moment

for this configuration and it is symmetric with respect to a rotation by π about the total angular momentum axis (rotational axis). The resulting quadrupole transition strength will decrease with the increase in spin along the band due to the gradual closing of the angular momentum blades.

Another type of regular band-like structure with different characteristic features but the same decreasing trend of $B(E2)$ values was observed for several nuclei in the mass $A \sim 110$ and 160 regions [17] and has been interpreted as smoothly terminating bands. These bands show the characteristic of gradually decreasing dynamic moments of inertia with increasing spin in contrast to a fairly constant dynamic moment of inertia (without any collective contribution) in the case of AMR [11]. The calculations show that these bands arise when a particular configuration evolves continuously from high collectivity at low spin to a point where all the spin vectors of the valence nucleons are aligned. With increasing spin, the intrinsic shape evolves until it is symmetric around the axis of rotation. Since collective rotation about the symmetry axis is forbidden, no further angular momentum can be generated and this represents termination of the rotational band. The difference between this mechanism and AMR is reflected in the variation of the dynamic moment of inertia [$J^{(2)}$] and $B(E2)$ strength as a function of spin. In the case of smoothly terminating bands, the ratio $J^{(2)}/B(E2)$ remains almost constant in contrast to a sharp increase in the case of an AMR [11] band.

The observation of a conjugate shear structure responsible for the generation of angular momentum in near spherical systems in the form of AMR is also associated with the possibility of a similar complementary excitation mode called magnetic rotation (MR) due to a single shear structure [16]. Indeed, different manifestations of the shears mechanism with single shear structure have been found in mass regions viz. $A \sim 80$, 100, 140 and 190 [18–27]. Since both of these two types of quantized rotation are the consequence of the shears mechanism, it is expected to observe both of them in all the mass regions mentioned above. However, until today, simultaneous occurrence of these two phenomena has been observed only in the mass ~ 100 region, where firm experimental evidence of AMR has been reported in several Cd [9–14] isotopes and in the ^{104}Pd nucleus [15] along with the observation of MR bands [22,23]. These bands have been interpreted in the framework of a simple geometric model [14,28,29] and as well as in the fully self-consistent microscopic tilted axis cranking method based on covariant density functional theory [30]. For the mass $A \sim 140$ region, the observed quadrupole band in ^{144}Dy [31] has been identified as a possible candidate for AMR on the basis of theoretical arguments. However, due to the absence of lifetime data, the nature of the excitation mechanism for this band cannot be firmly established as AMR.

In the present letter, the observation of an AMR band is reported for the ^{143}Eu nucleus. The AMR phenomenon in the present case has been established on the basis of the decreasing $B(E2)$ values with increasing spin for the band of interest. Furthermore, a sudden increase of the $B(E2)$ value, at higher spins, followed by another rapid decrease has been observed. This is the first nucleus to exhibit such a behavior and is a novel feature in the context of the AMR band.

The lifetimes of the excited states in ^{143}Eu have been measured using the Doppler shift attenuation method (DSAM). These states in the ^{143}Eu nucleus have been populated through the ^{116}Cd (^{31}P, 4n) reaction at a beam energy of 148 MeV. The beam was delivered by the Pelletron Linac Facility at the Tata Institute of Fundamental Research (TIFR), Mumbai. The target was 2.4 mg/cm^2 thick ^{116}Cd, enriched to 99%, on 14.5 mg/cm^2 Pb backing. The Indian National Gamma Array (INGA) [32,33], consisting of nineteen Compton-suppressed clover detectors, was used to detect the de-
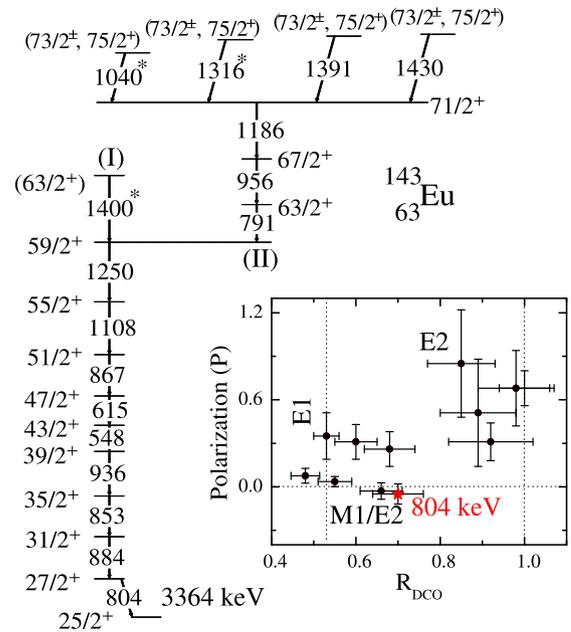

Fig. 1. (Color online.) The partial level scheme of the quadrupole structure in ^{143}Eu. The inset shows the variation of polarization vs DCO ratios (gate on $E2$ transitions) for different transitions in ^{143}Eu. The value for the 803.9-keV γ ray is represented by the filled red star. The level energy and gamma energies are rounded off to the nearest keV. The new transitions are indicated by an asterisk.

exciting γ rays. The experimental aspects and data analysis are detailed in Ref. [34].

The earlier studies on ^{143}Eu [35] reported a quadrupole cascade of $E2$ transitions, connected to the lower part of the level scheme by an 803.9-keV $E1$ transition. All the reported transitions [35] have been observed in the present measurements except for three new transitions which were placed in the partial level scheme [Fig. 1]. The values of the DCO ratio, anisotropy and linear polarization determined from the present experiment for the 803.9-keV transition have been found to be 0.70(0.06), 0.78(0.09) and −0.05(0.07), respectively [inset of Fig. 1]. These values conclusively establish that the 803.9-keV transition is of mixed character [with a 0.15(0.05) $M1/E2$ mixing ratio]. Thus, the reported $E2$ cascade has been identified as a positive parity sequence [Fig. 1]. In addition to the previously observed transitions, a weak 1400.0-keV transition parallel to 790.9-keV γ ray is observed above the 1249.7-keV transition. We have also observed two more weak transitions of energies 1316.0 and 1040.0 keV feeding the $71/2^+$ state. However, the spins and parities of the four states above $71/2^+$ could not be determined. Thus, all the possible assignments have been indicated in the partial level scheme [Fig. 1]. Fig. 2 shows the alignment plot for the quadrupole structure in ^{143}Eu which is indicative of a band crossing at a spin of $59/2^+$.

Doppler-broadened lineshapes have been observed for the transitions above the $I^\pi = 43/2^+$ state in ^{143}Eu. The level lifetimes of the states have been extracted by fitting these lineshapes using the LINESHAPE analysis code [37,38]. The slowing down history of 10,000 recoiling nuclei, traversing the target and the backing media, have been simulated by Monte Carlo techniques with a time step of 1.5 fs. The shell-corrected stopping powers of Northcliffe and Schilling [39] have been used for these calculations. These histories have been used to generate angle dependent velocity profiles for detectors at different angles wherein the clover geometry of the detector has been used as an input. The velocity profiles have been used to calculate Doppler shapes for the γ-ray transitions of interest. The experimental spectra have been constructed with gates on the γ-ray transitions below the band of interest.
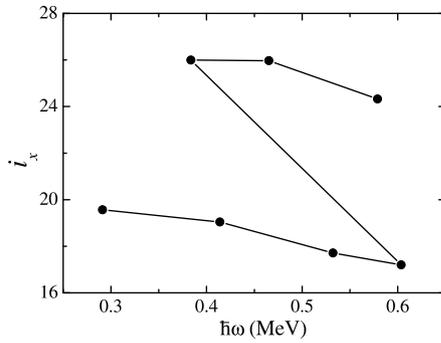
Fig. 2. Experimental aligned angular momentum (i_x) for the quadrupole structure (above $43/2^+$) in ^{143}Eu. The reference parameters were assumed to be $\mathcal{J}_0 = 12\hbar^2$ MeV^{-1} and $\mathcal{J}_1 = 25\hbar^4$ MeV^{-3}, adopted from Ref. [36].

The lifetimes for the states in the band have been extracted by least square fitting of the calculated shapes to the experimental (gated) spectra. The gate on the transitions below the transitions of interest necessitates to consider the side-feeding contribution. This has been modeled with a cascade of five transitions having the same moment of inertia as that of the band under consideration. Initially, starting from the topmost transition, the members of the band have been sequentially fitted. A direct feeding has been assumed to calculate the shape for the transition from the topmost level ($I^\pi = 71/2^+$) for which a clear lineshape has been observed. This gives us the value of the effective lifetime of the state. For the subsequent transitions in the band, the transition quadrupole moment, the side-feeding quadrupole moment, the peak height and the background have been used as free parameters for the least square procedure. Following a satisfactory fit, the spectrum parameters like the peak height and the background have been fixed at the corresponding values. After having fitted all the transitions of the band, sequentially, a global least square minimization has been carried out for all the transitions of the cascade, simultaneously, wherein only the transition quadrupole moments and the side-feeding quadrupole moments for each state have been kept as free parameters.

In the present work, the observed lineshapes at angles 65°, 90° and 140° have been fitted simultaneously to obtain the level lifetimes recorded in Table 1 along with the derived $B(E2)$ values. Representative lineshape fits are illustrated in Fig. 3. The uncertainties in the lifetimes have been derived from the behavior of the χ^2 fit in the vicinity of the minimum. The quoted errors in the lifetimes do not include the systematic error due to the un-
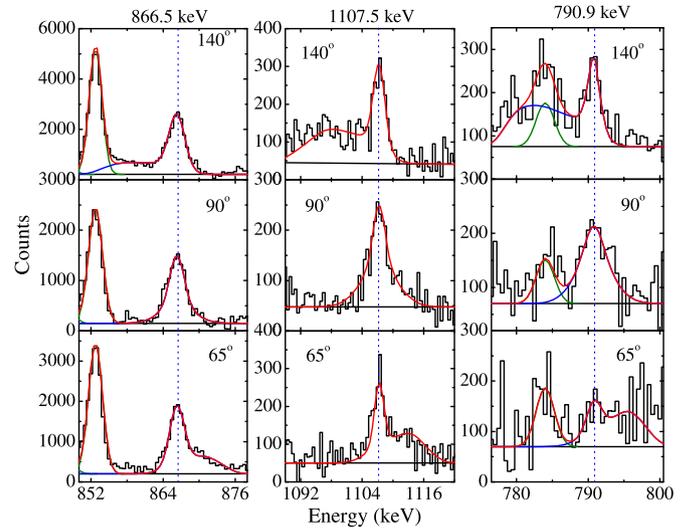
Fig. 3. (Color online.) Representative spectra along with theoretically fitted lineshapes for the quadrupole transitions at 866.5, 1107.5 and 790.9-keV of the quadrupole structure in ^{143}Eu. Calculated lineshape of γ transitions, contaminant peaks and total lineshapes are represented by the blue, olive and red curves, respectively.

certainty in the stopping power which can be as large as 15%. The level lifetimes have been evaluated in the present analysis by considering the side feeding from both observed as well as unobserved transitions to the level under consideration [23]. Thus, the lifetime for the $47/2^+$ state has been evaluated by including the 968.7-keV transition [35] in the feeding history parallel to the 866.5-keV transition. The 968.7-keV transition appears to be a fully stopped peak in the present experiment. For the next higher lying state at $51/2^+$, it was observed that the state was populated by a 697.9-keV transition ($53/2 \rightarrow 51/2^+$; not shown in Fig. 1) in addition to the 1107.5-keV transition also [35]. We have observed lineshapes for both these transitions in the experimental spectra. The partial lifetime for the $51/2^+$ state due to the feeding of 697.9-keV transition has been evaluated. In the final analysis, the top feed lifetime for the $51/2^+$ level was assumed to be the intensity weighted average of the lifetimes for $55/2^+$ and $53/2$ levels since this level was fed by both 1107.5-keV ($55/2^+ \rightarrow 51/2^+$) and 697.9-keV ($53/2 \rightarrow 51/2^+$) γ rays [40]. The side feeding intensity in all the levels was fixed to reproduce the observed intensity pattern at 90° with respect to the beam direction. The present analysis is validated by the close compliance of the lifetimes of

Table 1

Measured level lifetimes (τ) and the corresponding $B(E2)$ values for the quadrupole transitions in ^{143}Eu. The dynamic moment of inertia $J^{(2)}$ and the ratio of $J^{(2)}/B(E2)$ are also shown for the same transitions.

| Sequence	I_i^π [$\hbar$]	E_γ [keV]	τ[a] [ps]	τ[b] [ps]	$B(E2)$ [e²b²]	$J^{(2)}$ [$\hbar^2$ MeV^{-1}]	$J^{(2)}/B(E2)$ [$\hbar^2$ MeV^{-1}/(eb)²]
Structure I	$47/2^+$	614.8	3.1(3)	$2.76^{+0.42}_{-0.35}$	$0.34^{+0.05}_{-0.04}$	15.9	47^{+8}_{-7}
	$51/2^+$	866.5	0.6(2)	$0.66^{+0.14}_{-0.10}$	$0.25^{+0.05}_{-0.04}$	16.6	66^{+13}_{-11}
	$55/2^+$	1107.5	<0.5	$0.37^{+0.08}_{-0.06}$	$0.13^{+0.03}_{-0.02}$	28.1	216^{+50}_{-33}
	$59/2^+$	1249.7	<0.5	$0.44^{+0.06}_{-0.05}$	$0.06^{+0.01}_{-0.01}$	26.6	444^{+74}_{-74}
Structure II	$63/2^+$	790.9	<0.5	$0.48^{+0.08}_{-0.07}$	$0.35^{+0.06}_{-0.05}$d	24.3	69^{+12}_{-10}
	$67/2^+$	955.6	0.22(5)	$0.44^{+0.07}_{-0.05}$	$0.23^{+0.04}_{-0.03}$	17.4	76^{+13}_{-10}
	$71/2^+$	1185.7	<0.3	0.38c	$0.09\uparrow$	19.5	$216\downarrow$

a The level lifetimes are adopted from Ref. [35].
b Present measurements.
c Upper limit of level lifetime (τ).
d The 65% branching ratio for the 790.9 keV transition [35].
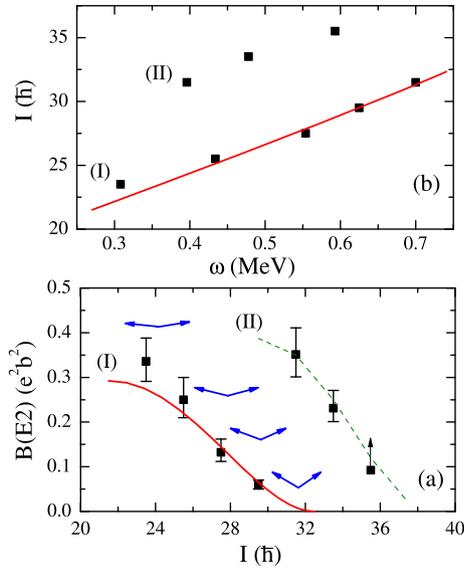
Fig. 4. (Color online.) Experimental (a) $B(E2)$ values with spin [$I(\hbar)$] and (b) $I(\hbar)$ against rotational frequency (ω) for the quadrupole band in ^{143}Eu. The solid red line represents the theoretical semi-classical particle plus rotor model calculation. The parameters used for this calculation are $V_{\pi\nu} = 1.7$-MeV, $V_{\pi\pi} = 0.2$-MeV, $j = 11/2$, $n = 10$, $a = 3.91$ and $|eQ_{eff}| = 1.40$ eb. The parameters have the same meaning as in Refs. [14,29]. The arrows depict the relative orientation of the $h_{11/2}$ proton blades for structure I. Theoretical $B(E2)$ values, represented by olive dash line ($j_h = 59/2\hbar$, $j_\pi = 9/2\hbar$ and $|eQ_{eff}| = 1.58$ eb), are calculated using Eq. (1) for structure II. The upward arrow in figure (a) represents the lower limit of $B(E2)$ value for the $71/2^+$ state of structure II.

the $47/2^+$ and $51/2^+$ states, measured in the present work, with those reported in Ref. [35]. For the states above the $51/2^+$ level, Ref. [35] only provided an upper limit on the lifetimes, except for the $67/2^+$ level.

Fig. 4(a) shows the variation of the deduced $B(E2)$ values with spin for the observed quadrupole band in ^{143}Eu. The $B(E2)$ values show a rapid decrease up to the state with spin-parity $59/2^+$ (marked as (I) in Fig. 4(a)). For the next higher lying state at $63/2^+$ it shows a sudden increase and again continues to decrease along the band (marked as (II) in Fig. 4(a)). The rapid increase of the $J^{(2)}/B(E2)$ ratios with increasing spins (Table 1) before the band crossing clearly excludes the possibility of structure I having a smoothly terminating origin. The trend of the $B(E2)$ values and the $J^{(2)}/B(E2)$ ratios are the definitive experimental signatures for the AMR phenomenon as far as structure I is concerned. This can be viewed as conclusive evidence for an AMR interpretation of structure I and places it on equal footing with observations in the $A \sim 100$ region. The behavior of structure II will be discussed later.

The ^{143}Eu ($Z = 63$, $N = 80$) nucleus has one proton hole and two neutron holes with respect to the semi-magic nucleus ^{146}Gd. However, protons can be easily excited to the $h_{11/2}$ orbital across $Z = 64$ subshell closure, leading to the observation of the MR bands. Such bands have been observed in the neighboring ^{142}Sm, ^{141}Eu, ^{142}Gd nuclei, which were interpreted in the framework of the tilted axis cranking and the shears mechanism with the principal axis cranking model using a small oblate deformation [34,41,42].

In contrast to the previous work [35], we have assigned the configuration $(\nu h_{11/2}^{-2} \pi (d_{5/2}/g_{7/2})^{-3})_{37/2} \otimes (\pi h_{11/2}^2)_0$ to the $43/2^+$ state (the previous assignment was $\pi (d_{5/2}^{-1} g_{7/2}^{-1} h_{11/2}) \nu h_{11/2}^{-2}$). This is due to the fact that for oblate deformation, three proton holes in the $d_{5/2}/g_{7/2}$ orbitals, being rotation aligned, along with two neutron holes in the $h_{11/2}$, produce a total angular momentum

of $37/2^+$. This is close to the bandhead spin of $43/2^+$ for the proposed AMR band (structure I). The difference ($3\hbar$) can be attributed to the contribution of the core. On the other hand, the two protons in the time reversed $h_{11/2}$ orbitals produce two angular momentum vectors which are anti-aligned to each other and perpendicular to the total angular momentum of the rotation-aligned holes. Thus, for this configuration, the double shear structure can exist. We have calculated the bandhead energy for the above configuration using a particle hole calculation in the relativistic mean field approach [43] using the blocked BCS method. The calculated energy of the bandhead is found to be 6.8 MeV, whereas the corresponding observed value is 7.4 MeV. The difference may be due to the effect of core rotation which is not considered in the present relativistic mean field calculations. It has also been observed from the calculations that the potential energy surfaces for the seven quasi-particle state is much deeper (~ 700 keV) for oblate deformation compared to prolate one.

In order to explore the possibility of an AMR band in ^{143}Eu for the above mentioned configuration, we have performed a numerical calculation within the framework of a self-consistent semi-classical rotor plus shears model [14,29] based on the proton–neutron residual interaction [44]. In this model the total energy of an excited state is the sum of the rotational energy of the weakly deformed core and the effective interaction energy between the shears blades. The transition probability of the state in the anti-magnetic shear can be expressed as [14,29],

$$B(E2) = \frac{15}{32\pi} (eQ_{eff})^2 \sin^4\theta \qquad (1)$$

where θ is the angle between the rotational axis and any one of the proton angular momentum vectors.

Experimental $I(\omega)$ values have been compared with the calculations from the semi-classical rotor plus shears model in Fig. 4(b). The good agreement seems to indicate that structure I originates from AMR with the configuration $\nu h_{11/2}^{-2} \pi (d_{5/2}/g_{7/2})^{-3} \otimes \pi h_{11/2}^2$. In order to validate this proposition, the $B(E2)$ values have been computed using Eq. (1) where the shears angle for each angular momentum state has been calculated from the semi-classical model. These values are represented by the solid line in Fig. 4(a). This agreement provides the essential self-consistency check. The quadrupole deformation parameter corresponding to the value of $|Q_{eff}|$ used in the semi-classical calculation for structure I is ~ 0.08. This is consistent with a general picture where AMR only occurs for small deformation. The presence of the 1400.0-keV transition above the $59/2^+$ state may indicate the termination of the band at a spin $63/2^+$ state due to the complete alignment of two $h_{11/2}$ protons leading to an angular momentum gain of $10\hbar$. Thus, the present calculations seems to indicate that sequence I originates from the AMR in an oblate nucleus with small deformation. This is a unique observation since all the nuclei in the $A \sim 100$ region where the AMR has been established, are prolate.

It has been observed from Fig. 4(a) that there is a large increase of the $B(E2)$ value at a spin of $63/2^+$. The nature of this variation in the $B(E2)$ value, a unique feature of the current observation, has not been observed in any nucleus. However, such a sudden increase in $B(M1)$ values has been observed in different mass regions and has been interpreted as a crossing of two MR bands [19,45,46]. Thus, the observation may possibly be associated with the emergence of a new double shear structure. This possibility is also supported by the fact that the original AMR structure can generate spin only upto $63/2^+$ and the observed states with higher angular momentum must have a different single particle configuration, resulting in a re-opening of the shear structure. A new configuration $[\nu h_{11/2}^{-2} \pi (d_{5/2}/g_{7/2})^{-3} \pi h_{11/2}^2 + core(3\hbar)]_{59/2} \otimes \pi h_{11/2}^2$ has been tentatively assigned for the quadrupole structure II where

two additional $h_{11/2}$ protons in time reversed orbits start to align. This is in addition to the rotation aligned spin (59/2) due to structure I. The coupling of these angular momentum vectors may be visualized as another double shear like structure responsible for the generation of a different AMR band with a new shear angle.

We have performed a semiclassical model calculation with the proposed configuration for structure II, though the AMR interpretation remains tentative for this structure. The results reproduced the experimental $B(E2)$ values for structure II (Fig. 4(a)). However, this agreement is limited to the two experimental values since only the lower limit of $B(E2)$ value could be estimated from the effective lifetime of the $71/2^+$ state. For this calculations we have assumed that the proton blades are not fully stretched. Such non-stretched configurations have been assumed in semiclassical calculations [34,41,42] in this mass region. The structure II is also found to be weakly deformed with deformation parameter $|\beta_2| \sim 0.09$ corresponding to $|eQ_{eff}| = 1.58$ (figure caption of Fig. 4). In these calculations, the values of shears angle (θ) are obtained directly from the relation $I = j_h + 2j_\pi \cos\theta$ for the assumed configuration where j_h is the total angular momentum of the quasi-particles aligned along the rotational axis at the bandhead and the angular momentum assumed due to the rotation of the core. In this case the maximum spin that can be generated due to the alignment of two more protons in the $h_{11/2}$ orbital is $6\hbar$ because of Pauli blocking (as two protons are already aligned corresponding to the projection 11/2 and 9/2 for sequence I, the available projected states for the next pair of $h_{11/2}$ protons are 7/2 and 5/2) and hence, this band is expected to generate a maximum spin of $71/2^+$ which is corroborated by the experimental results. The presence of high-energy transitions above the state at $71/2^+$ may represent the termination of the AMR band. However, the increasing trend of the $J^{(2)}/B(E2)$ ratios for structure II [Table 1] cannot be definitely ascertained from the present experimental data. Hence, the possibility of smooth band termination for structure II cannot be excluded [17]. Thus, no firm interpretation could be given to structure II from the present measurements.

In summary, the high spin quadrupole structure in ^{143}Eu has been investigated using the reaction ^{116}Cd (^{31}P, 4n) at a beam energy of 148 MeV. The level lifetimes in the quadrupole structure have been measured. The deduced $B(E2)$ values decrease with increasing spin (and there is also an increase of $J^{(2)}/B(E2)$ values), indicating the band (structure I) to be of AMR origin, followed by a sudden increase at spin-parity $63/2^+$. The configuration $\nu h_{11/2}^{-2} \pi(d_{5/2}/g_{7/2})^{-3} \otimes \pi h_{11/2}^2$ has been assigned to structure I from the semi-classical model calculations, which clearly show that the quadrupole band (structure I) in ^{143}Eu originates from AMR. For structure II, a tentative configuration of $[\nu h_{11/2}^{-2} \pi(d_{5/2}/g_{7/2})^{-3} \pi h_{11/2}^2 + core(3\hbar)]_{59/2} \otimes \pi h_{11/2}^2$ has been assigned. The $B(E2)$ values for the states in quadrupole structure II have been reproduced well within the framework of a semi-classical shears model from which it may be concluded that this band may also originate from AMR, but the possibility of smooth band termination can not be ruled out. The sudden rise of the $B(E2)$ value at $63/2^+$ may be due to crossing of the two AMR bands. However, such band crossing phenomenon is not incorporated in the present semi-classical model [14,29]. Detailed investigation in the framework of a microscopic model may lead to a better understanding of this behavior. The present measurements conclusively establish AMR in the $A \sim 140$ region. This observation outside the $A \sim 100$ region establishes the AMR phenomenon as an alternative mechanism for generation of high angular momentum states in weakly-deformed nuclei.

Acknowledgements

References

[1] A. Bohr, B.R. Mottelson, Phys. Rev. 90 (1953) 717.
[2] S. Raman, C.W. Nestor Jr, P. Tikkanen, At. Data Nucl. Data Tables 78 (2001) 1.
[3] N.J. Stone, At. Data Nucl. Data Tables 90 (2005) 75.
[4] A. Bohr, B.R. Mottelson, Nuclear Structure Vol. II, Benjamin, 1975.
[5] C.J. Chiara, et al., Phys. Rev. C 61 (2000) 034318.
[6] M. Sugawara, et al., Phys. Rev. C 86 (2012) 034326.
[7] P.H. Regan, et al., Nucl. Phys. A 586 (1995) 351–376.
[8] S. Zhu, et al., Phys. Rev. C 64 (2001) 041302(R).
[9] A.J. Simons, et al., Phys. Rev. Lett. 91 (2003) 162501.
[10] P. Datta, et al., Phys. Rev. C 71 (2005) 041305(R).
[11] A.J. Simons, et al., Phys. Rev. C 72 (2005) 024318.
[12] Deepika Choudhury, et al., Phys. Rev. C 82 (2010) 061308(R).
[13] Deepika Choudhury, et al., Phys. Rev. C 87 (2013) 034304.
[14] Santosh Roy, et al., Phys. Lett. B 694 (2011) 322.
[15] N. Rather, et al., Phys. Rev. C 89 (2014) 061303(R).
[16] S. Frauendorf, Rev. Mod. Phys. 73 (2001) 463.
[17] A.V. Afanasjev, et al., Phys. Rep. 322 (1999) 1.
[18] G. Baldsiefen, et al., Z. Phys. A 355 (1996) 337–338.
[19] Priyanka Agarwal, et al., Phys. Rev. C 76 (2007) 024321.
[20] S. Lakshmi, et al., Phys. Rev. C 69 (2004) 014319.
[21] D.G. Jenkins, et al., Phys. Rev. C 58 (1998) 2703.
[22] N.S. Kelsall, et al., Phys. Rev. C 61 (1999) 011301(R).
[23] P. Datta, et al., Phys. Rev. C 69 (2004) 044317.
[24] R. Schwengner, et al., Phys. Rev. C 65 (2002) 044326.
[25] R. Schwengner, et al., Phys. Rev. C 80 (2009) 044305.
[26] Amita, A.K. Jain, B. Singh, At. Data Nucl. Data Tables 74 (2000) 283.
[27] H. Hübel, Prog. Part. Nucl. Phys. 54 (2005) 1.
[28] R.M. Clark, A.O. Macchiavelli, Annu. Rev. Nucl. Part. Sci. 50 (1) (2000).
[29] S. Roy, S. Chattopadhyay, Phys. Rev. C 83 (2011) 024305.
[30] P.W. Zhao, J. Peng, H.Z. Liang, P. Ring, J. Meng, Phys. Rev. Lett. 107 (2011) 122501.
[31] M. Sugawara, et al., Phys. Rev. C 79 (2009) 064321.
[32] R. Palit, et al., Nucl. Instrum. Methods A 680 (2012) 90.
[33] R. Palit, et al., J. Phys. Conf. Proc. 420 (2013) 012159.
[34] S. Rajbanshi, et al., Phys. Rev. C 89 (2014) 014315.
[35] M. Piiparinen, et al., Nucl. Phys. A 605 (1996) 191–268.
[36] D.M. Cullen, et al., Phys. Rev. C 66 (2002) 034308.
[37] J.C. Wells, N.R. Johnson, LINESHAPE: a computer program for doppler broadened lineshape analysis, Report No. ORNL-6689, 44, 1991.
[38] N.R. Johnson, et al., Phys. Rev. C 55 (1997) 652.
[39] L.C. Northcliffe, R.F. Schilling, At. Data Nucl. Data Tables A 7 (1970) 233.
[40] N. Rather, et al., Phys. Rev. Lett. 112 (2014) 202503.
[41] E.O. Podsvirova, et al., Eur. Phys. J. A 21 (2004) 1–6.
[42] A.A. Pasternak, et al., Eur. Phys. J. A 23 (2005) 191–196.
[43] R. Raut, et al., Phys. Rev. C 73 (2006) 044305.
[44] A.O. Macchiavelli, et al., Phys. Rev. C 57 (1998) R1073(R).
[45] R.M. Clark, et al., Phys. Rev. Lett. 78 (1997) 1868.
[46] Santosh Roy, et al., Phys. Rev. C 81 (2010) 054311.